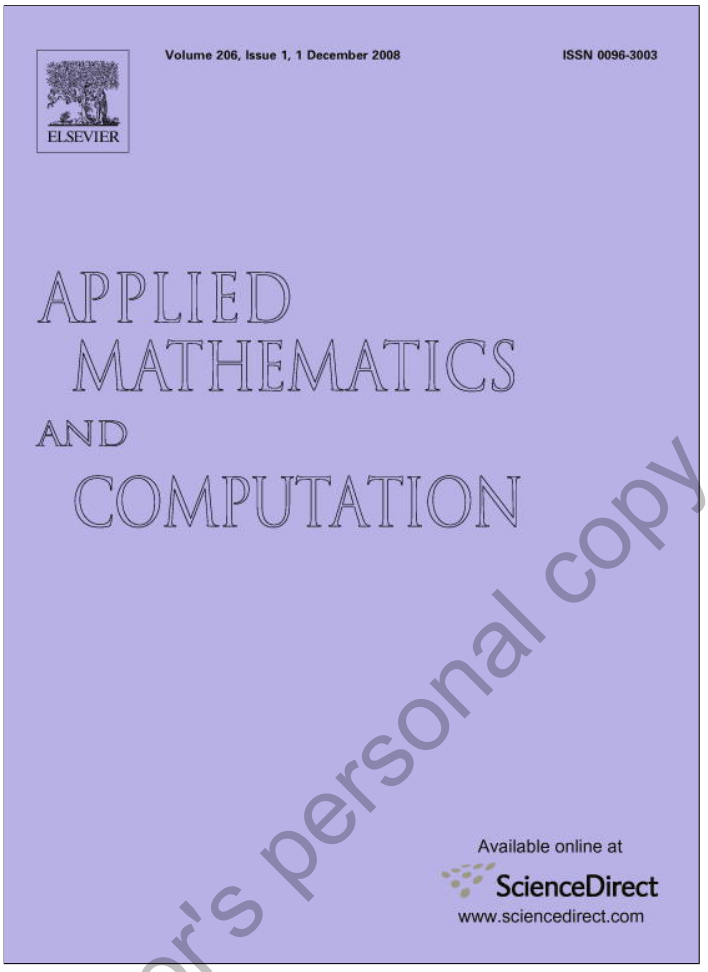

Applied Mathematics and Computation 206 (2008) 205–213

Contents lists available at ScienceDirect

Applied Mathematics and Computation

journal homepage: www.elsevier.com/locate/amc

A consistent boundary condition for vorticity–streamfunction simulation of wall-bounded vortex flow

Z.C. Zheng

Department of Mechanical and Nuclear Engineering, Kansas State University, Manhattan, KS 66506, United States

ARTICLE INFO

Keywords:
Vorticity–streamfunction simulation
Vortex flow
Vorticity boundary conditions

ABSTRACT

This paper was motivated by a computational effort to model the aircraft wake vortex hazard near airports. Those flows can usually be approximated as a pair of two-dimensional, incompressible vortices interacting with an infinite solid wall. The present numerical model uses a vorticity–streamfunction formulation to simulate the two-dimensional problem. Since vorticity generation near the wall alters the evolution of the secondary and tertiary vortices directly, accurate modeling of the wall region is critical. A local relationship between vorticity and streamfunction for a wall boundary condition has been established from a new point of view, by specifying the streamfunction at the boundary grid lifted away from the solid wall. The new method has utilized Taylor series expansions near the wall boundary. Although the resulting expressions are only first order accurate, the critical importance of physical and mathematical consistency has been achieved. Numerical test cases are discussed in the paper.

1. Introduction

Vortex interactions with a rigid wall have been studied via computational fluid dynamics for a variety of different applications [1]. For example, the behavior of aircraft trailing vortices with ground effects, and small scale vortices in a boundary layer. This paper was motivated by a computational effort to model the aircraft wake vortex hazard near airports. The primary purpose was to calculate the trajectories and strengths of the wake vortex pair near the ground. Those flows can usually be approximated as a pair of two-dimensional, incompressible vortices interacting with an infinite solid wall (Fig. 1). However, the wall boundary layer region can include separated flows induced by the vortex pair [2] and can generate secondary and tertiary vortices. Subsequently, the interaction between the primary vortices and the newly-formed secondary and tertiary vortices influences the behavior of the vortex pair significantly. The present numerical model uses a vorticity–streamfunction formulation, because of its obvious simplicity in the two-dimensional problem. However, since vorticity generation near the wall alters the evolution of the secondary and tertiary vortices, accurate modeling of the wall region is critical. The fundamental issue for accurate numerical simulation is the solid wall vorticity boundary conditions, as discussed in a series of review articles by Gresho [3–5]. That is the focus of this paper.

Anderson [6] classified three techniques that could be used for overcoming the difficulties associated with the numerical implementation of vorticity boundary conditions. The *vorticity–streamfunction* approach includes those schemes which exploit the relationship between the vorticity and the streamfunction, as described in [7–9]. The second technique requires that the vorticity should evolve subject to an *integral constraint*, as proposed in [10] and used, with its time derivative, in [6]. The third class is often called *vortex blob* methods and was originally introduced in [11]. The present study has developed a staggered grid technique to yield a simple specific boundary condition on vorticity, while avoiding over-specification of the

E-mail address: zzheng@ksu.edu

0096-3003/$ - see front matter © 2008 Elsevier Inc. All rights reserved.
doi:10.1016/j.amc.2008.09.012

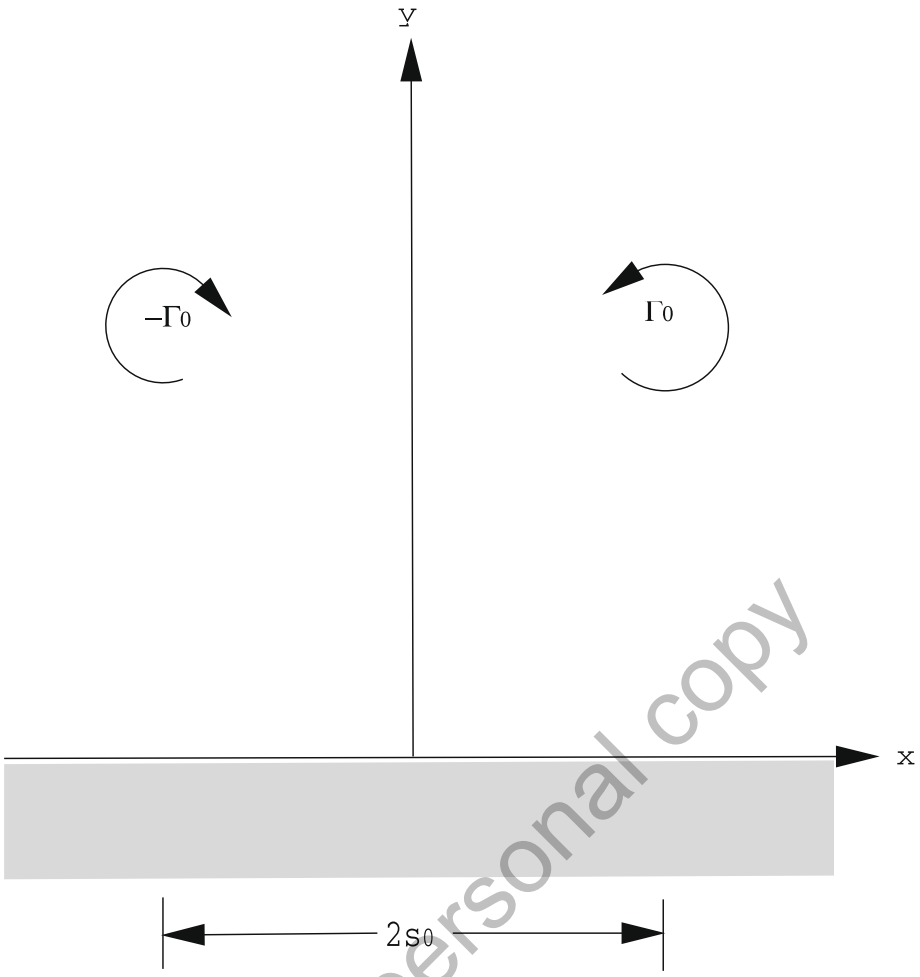

Fig. 1. Coordinate system used in this study.

streamfunction boundary condition at the wall. The approach can be classified as a type of vorticity–streamfunction relationship, among the approaches described above.

The new method has utilized Taylor series expansions near the wall boundary. The resultant boundary condition is a local relationship between vorticity and streamfunction, which is a natural approach when using finite difference methods. However, an undistorted relationship is important near the solid boundary. The present method enforces the physical velocity boundary condition by specifying the streamfunction at the boundary-adjacent grid locations, which are thus lifted away from the wall boundary. The vorticity levels at those points are then related to the streamfunction without direct knowledge of the velocity. With that procedure, over-specification of the streamfunction is avoided, while the physical velocity boundary condition is enforced numerically. Even though the resulting expressions are only first order accurate, they still satisfy the only Neumann type physical boundary condition and therefore the critical requirement of physical and mathematical consistency has been achieved.

In the next section, the solid wall vorticity boundary condition will be discussed. Then, the numerical grid and scheme will be briefly explained in Section 3 and in Section 4 the numerical test cases that have been performed will be discussed.

2. Vorticity boundary condition

It is noted that in the vorticity–streamfunction formulation, only streamfunction and vorticity are calculated on numerical grid points, while velocities, which are the first derivatives of streamfunction, are not. Following the ideas of staggered grids, the odd derivatives can only be satisfied approximately on a staggered grid if the computation is based on even derivative variables. Since realistic physical boundary conditions are only related to velocity on the ground boundary, they cannot be specified accurately using the vorticity–streamfunction formulation. That is why some vorticity boundary conditions, which require an *a priori* accurate velocity boundary condition, give erroneous results.

For example, if a Taylor series expansion is used on the grid points adjacent to the ground, we have

$$\psi(h_1) = \psi_W + h_1 \left.\frac{\partial \psi}{\partial y}\right|_{y=0} + \frac{h_1^2}{2} \left.\frac{\partial^2 \psi}{\partial y^2}\right|_{y=0} + O(h_1^3), \tag{1}$$

where ψ_W is the streamfunction value on the ground, which can be set to zero for the non-penetration boundary, and h_1 is the vertical spacing of the first grid away from the ground. On the ground, we also have

$$\zeta_W = -\left(\frac{\partial^2\psi}{\partial x^2} + \frac{\partial^2\psi}{\partial y^2}\right)\bigg|_{y=0} = -\frac{\partial^2\psi}{\partial y^2}\bigg|_{y=0}. \tag{2}$$

Hence, from Eqs. (1) and (2), we obtain the ground boundary vorticity

$$\zeta_W = -\frac{2\psi(h_1)}{h_1^2} + \frac{2}{h_1}\frac{\partial\psi}{\partial y}\bigg|_{y=0} + O(h_1). \tag{3}$$

It appears that since $\psi(h_1)$ is on the interior points, which can be calculated, and $\partial\psi/\partial y(y=0)$ can be determined by the no-slip condition, $\partial\psi/\partial y(y=0) = u_W$, the vorticity values on the wall boundary can be obtained. However, it must be noted that if the velocity boundary condition cannot really be satisfied numerically in the vorticity–streamfunction calculation, the second term on the right-hand-side of Eq. (3) can produce errors. The magnitude of those errors depends on the uncontrollable accuracy of the actual numerical derivatives of streamfunction at the wall; but they are always amplified by $1/h_1$. When $h_1 \to 0$, the "fine grid nightmare", mentioned in [4] can occur.

Since the boundary conditions for vorticity and streamfunction should not be given at the same boundaries as velocity, in the following approach, we shift the computational domain from the wall. Fig. 2 shows the grid near the wall boundary, where the grid for streamfunction and vorticity is assumed to be staggered over the velocity grid. The shifted distance, αh_1, will be determined, in order to produce a proper relationship between vorticity and streamfunction.

At $y = \alpha h_1$ and $y = \alpha h_1 + h_1$, Taylor series expansions are used to write:

$$\psi_1 = \psi(\alpha h_1) = h_1\frac{\partial\psi}{\partial y}\bigg|_{y=0} + \frac{h_1^2}{2}\frac{\partial^2\psi}{\partial y^2}\bigg|_{y=0} + \frac{h_1^3}{3}\frac{\partial^3\psi}{\partial y^3}\bigg|_{y=0} + O(h_1^4), \tag{4}$$

$$\psi_2 = \psi(\alpha h_1 + h_1) = (\alpha h_1 + h_1)\frac{\partial\psi}{\partial y}\bigg|_{y=0} + \frac{(\alpha h_1 + h_1)^2}{2}\frac{\partial^2\psi}{\partial y^2}\bigg|_{y=0} + \frac{(\alpha h_1 + h_1)^3}{6}\frac{\partial^3\psi}{\partial y^3}\bigg|_{y=0} + O(h_1^4), \tag{5}$$

and

$$\zeta_1 = \zeta(\alpha h_1) = \zeta_W + \alpha h_1\frac{\partial\psi}{\partial y}\bigg|_{y=0} + O(h_1^2). \tag{6}$$

From the Poisson equation for streamfunction, we have Eq. (2) and

$$\frac{\partial\zeta}{\partial y}\bigg|_{y=0} = -\left[\frac{\partial^2}{\partial x^2}\left(\frac{\partial\psi}{\partial y}\bigg|_{y=0}\right) + \frac{\partial^3\psi}{\partial y^3}\bigg|_{y=0}\right]. \tag{7}$$

From Eqs. (2), (6) and (7), we obtain

$$\zeta_1 = -\frac{\partial^2\psi}{\partial y^2}\bigg|_{y=0} - \alpha h_1\frac{\partial^3\psi}{\partial y^3}\bigg|_{y=0} - \alpha h_1\frac{\partial^2}{\partial x^2}\left(\frac{\partial\psi}{\partial y}\bigg|_{y=0}\right) + O(h_1^2). \tag{8}$$

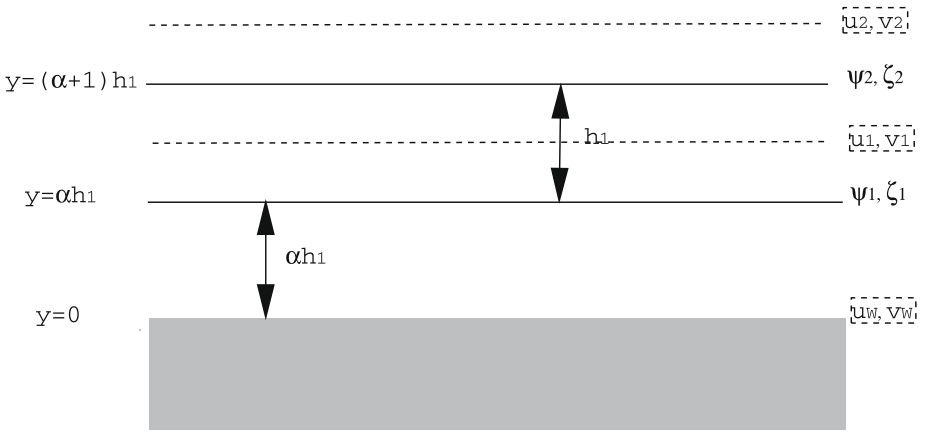

Fig. 2. Staggered grid near the wall boundary.

The linear combination of ζ_1, ψ_1, and ψ_2 is

$$h_1^2\zeta_1 + p_1\psi_1 + p_2\psi_2 = [p_1\alpha + p_2(1+\alpha)]h_1\left.\frac{\partial\psi}{\partial y}\right|_{y=0} + \left[p_1\frac{\alpha^2}{2} + p_2\frac{(1+\alpha)^2}{2} - 1\right]h_1^2\left.\frac{\partial^2\psi}{\partial y^2}\right|_{y=0} \times \left[p_1\frac{\alpha^3}{6} + p_2\frac{(1+\alpha)^3}{5} - \alpha\right]h_1^3\left.\frac{\partial^3\psi}{\partial y^3}\right|_{y=0} - \alpha h_1^3\frac{\partial^2}{\partial x^2}\left(\left.\frac{\partial^2\psi}{\partial y^2}\right|_{y=0}\right) + O(h_1^4). \tag{9}$$

If we want to develop a vorticity boundary condition without specifying the unknown derivatives of streamfunction on the solid wall, which are $\partial^n\psi/\partial y^n(y=0)$ for $n = 1$, 2 and 3, we need to have

$$\begin{cases} \alpha(p_1+p_2) + p_2 = 0, \\ \alpha^2 p_1 + (1+\alpha)^2 p_2 = 2, \\ \alpha^3 p_1 + (1+\alpha)^3 p_2 = 6\alpha. \end{cases} \tag{10}$$

Solving the equation set Eq. (10) for α, p_1 and p_2, we obtain $\alpha = 1$, $p_1 = -2$, and $p_2 = 1$. Therefore, Eq. (9) gives

$$\zeta_1 = -\frac{\psi_2 - 2\psi_1}{h_1^2} - h_1\frac{\partial^2}{\partial x^2}\left(\frac{\partial^2\psi}{\partial y^2}|_{y=0}\right) + O(h_1^2). \tag{11}$$

In Eq. (11), the second term still has the first derivative of streamfunction in it, which will be determined later. However, now $\partial\psi/\partial y(y=0)$ only has an $O(h_1)$ effect on the vorticity boundary condition, rather than an $O(1/h_1)$ effect, as in Eq. (3). Eq. (4) is then used to determine how the velocity condition can be satisfied. If we define

$$\psi_1 \equiv h_1 u_W, \tag{12}$$

from Eq. (4), we have

$$\left.\frac{\partial^2\psi}{\partial y^2}\right|_{y=0} = u_W + O(h_1). \tag{13}$$

Substituting into Eq. (11), we obtain the vorticity boundary condition

$$\zeta_1 = -\frac{\psi_2}{h_1^2} - \frac{2u_W}{h_1} - h_1\frac{\partial^2}{\partial x^2}(u_W + O(h_1)) + O(h_1^2) = -\frac{\psi_2}{h_1^2} - \frac{2u_W}{h_1} + O(h_1^2). \tag{14}$$

It is noted that although Eq. (14) gives a formal second order vorticity boundary condition, the effective boundary condition is only first order, because of the first order velocity boundary condition in Eq. (13). With the special case in this study, $u_W = 0$, the above boundary conditions become:

$$\zeta_1 = -\frac{\psi_2}{h_1^2}, \quad \psi_1 = 0. \tag{15}$$

Since the velocity and streamfunction boundary conditions cannot be specified at the same boundary, the present method enforces the physical velocity boundary condition by specifying the streamfunction at the first grid position, which is lifted away from the wall boundary. The vorticities at those points are then related to the streamfunction in the same Poisson equation relationship as for the interior points, without knowledge of the velocity. With that procedure, over-specification of the streamfunction is avoided, while the physical velocity boundary condition is enforced numerically. It was noted that those expressions are only first order accurate. However, higher order accuracy is difficult to maintain near the boundary for any numerical scheme. Hence, the actual computational domain is shifted h_1 away from the wall and with the clustered grid near the wall, the $O(h_1)$ truncation effect on the entire calculation can be constrained by the grid size employed at the first grid location along the wall, and can thus be set to a very small value, for the purpose of resolving the wall boundary layer. The uncontrollable first order derivative terms in Eq. (3) are canceled in the procedure and consistency can be satisfied with grid refinement.

It has also been noted that Eq. (15) was listed as an $O(1)$ accurate vorticity boundary condition in [9]. However, Anderson [12] used the same boundary condition to verify the equivalence between that boundary condition and the vorticity generation type boundary condition for the Stokes boundary value problem. He also pointed out that Eq. (15) gave first order accuracy. Numerical tests will be given on the current boundary condition and the first and second order vorticity boundary conditions listed in [9] which will demonstrate the superiority of the boundary condition given in Eq. (15).

3. Computational grid and scheme

In this study, a fixed grid was used rather than an unsteady, adaptive grid, due to the complexity of the vortex trajectories when in ground effect, resulting therefore in a lack of *a priori* knowledge of the locations requiring fine grid zones. Since the problem is symmetric with respect to the y-axis, it was only necessary to consider the first quadrant. However, the elliptic

character of the incompressible flow field mandates either enforcing the boundary conditions at the infinite limits of x and y or alternatively the development of rigorous boundary condition approximations within a finite domain [13,14].

To avoid the difficulties in specifying the boundary conditions at the infinite limits, the exponential transformation used in [15] was redeveloped as an adjustable transformation which transformed the physical domain to the computational domain, according to

$$X = a(1 - e^{-bx}), \quad Y = c(1 - e^{-dy}), \tag{16}$$

thus mapping $0 \leqslant x \leqslant \infty$, $0 \leqslant y \leqslant \infty$ into the finite domain $0 \leqslant X \leqslant a$, $0 \leqslant Y \leqslant c$, and permitting the distribution of densely packed grid points near the ground plane, while stretching the grid spacing as the infinite limits are approached. The resolution of boundary layer and vortex core was controlled by adjusting the arbitrary constants a, b, c and d.

As a representative example, when the initial vortex core radius was $r_c = 0.2$, we required $\Delta y_{max} = 0.02\ (= r_c/10)$ at the start-up altitude, y_0, and $\Delta x_{max} = 0.1\ (= r_c/2)$ at x_l, a position where the vortex core is at the greatest horizontal distance from the symmetry plane. The Δx_{max} spacing was more compact relative to the vortex core, due to dilation beginning from $t = 0$. By taking the derivatives of Eq. (16), we have $\Delta X \approx abe^{-bx}\Delta x$ and $\Delta Y \approx cde^{-dy}\Delta y$. Notice $M\Delta X = a$ and $N\Delta Y = b$, where M and N are the numbers of grid in the X and Y directions, respectively. Hence, it can be proved that the minimum number of grid points in each direction for acceptable resolution occurs when $b = 1/x_l$ and $d = 1/y_0$, and is given by

$$M \geqslant 10x_l e, \quad N \geqslant 50y_0 e. \tag{17}$$

The non-dimensional vorticity–streamfunction formulation in the transformed domain, made dimensionless using the initial vortex pair half-span, x_0, and the initial circulation, Γ_0, is represented by

$$\frac{\partial Q}{\partial t} + \frac{\partial (E - E_v)}{\partial t} + \frac{\partial (F - F_v)}{\partial t} = 0, \tag{18}$$

where

$$\begin{aligned} Q &= \frac{\zeta}{bd(a - X)(c - Y)}, \quad E = \frac{\partial \psi}{\partial Y}\zeta, F = -\frac{\partial \psi}{\partial X}\zeta, \\ E_v &= \frac{1}{Re}\frac{b(a - X)}{d(c - Y)}\frac{\partial \zeta}{\partial X}, \quad F_v = \frac{1}{Re}\frac{d(c - Y)}{b(a - X)}\frac{\partial \zeta}{\partial Y}. \end{aligned} \tag{19}$$

The convection terms give the Jacobian,

$$J(\zeta, \psi) = \frac{\partial E}{\partial X} + \frac{\partial F}{\partial Y} = \frac{\partial \zeta}{\partial X}\frac{\partial \psi}{\partial Y} - \frac{\partial \zeta}{\partial Y}\frac{\partial \psi}{\partial X}, \tag{20}$$

which can easily be proved to have the properties required for Arakawa's quadratic conservative algorithm, as shown in [16]. However, it should be noted that with viscous effects, neither vorticity nor the quadratic quantities (the total entropy and kinetic energy) are conserved. In addition, even in inviscid flows, the quadratic conservative scheme is accurate when periodic boundary conditions are used. Here, the Arakawa scheme is used for the purpose of reducing the dissipation and dispersion errors caused by the discretization of the convection terms, so that the physical diffusion effects can be mimicked accurately by the numerical scheme.

Quadratic conservation requirements are not important in low Reynolds number calculations, as in [15], because numerical diffusion from the convection terms is much smaller in comparison with the real diffusion terms, thus the high frequency components caused by the nonlinear effects can be suppressed by the high dissipation. For high Reynolds number flows, physical diffusion is small and therefore the numerical diffusion for the convection terms needs to be limited in order to avoid distortion of the solutions. However, since the boundary conditions and viscous effects cannot conserve the quadratic quantities, the second order, 9-point, central-differencing Arakawa scheme, applied through $J(\zeta, \psi)$ in the transformed domain, can still generate high frequency components. If the Reynolds number is very high, the physical dissipation is not sufficient to damp the high frequency waves. Hence, for very high Reynolds number flows ($Re \geqslant 10^{-4}$), Leonard's [17] third order smoothing was used to suppress the nonlinear instabilities.

The linear stability of the scheme is guaranteed by using a hopscotch time marching procedure, with time steps restricted by

$$\Delta t < \frac{\Delta x^2}{2}Re, \quad \Delta t < \frac{\Delta x}{U_{max}}. \tag{21}$$

The Poisson equation for the streamfunction can be solved efficiently using the Poisson solver, developed in [18] via spectral methods.

4. Numerical tests and discussion

The vorticity boundary condition has been tested to compare with an asymptotic solution developed by Zheng [18] for the initial boundary layer at the wall induced by a pair of vortices. The first and second order vorticity boundary conditions,

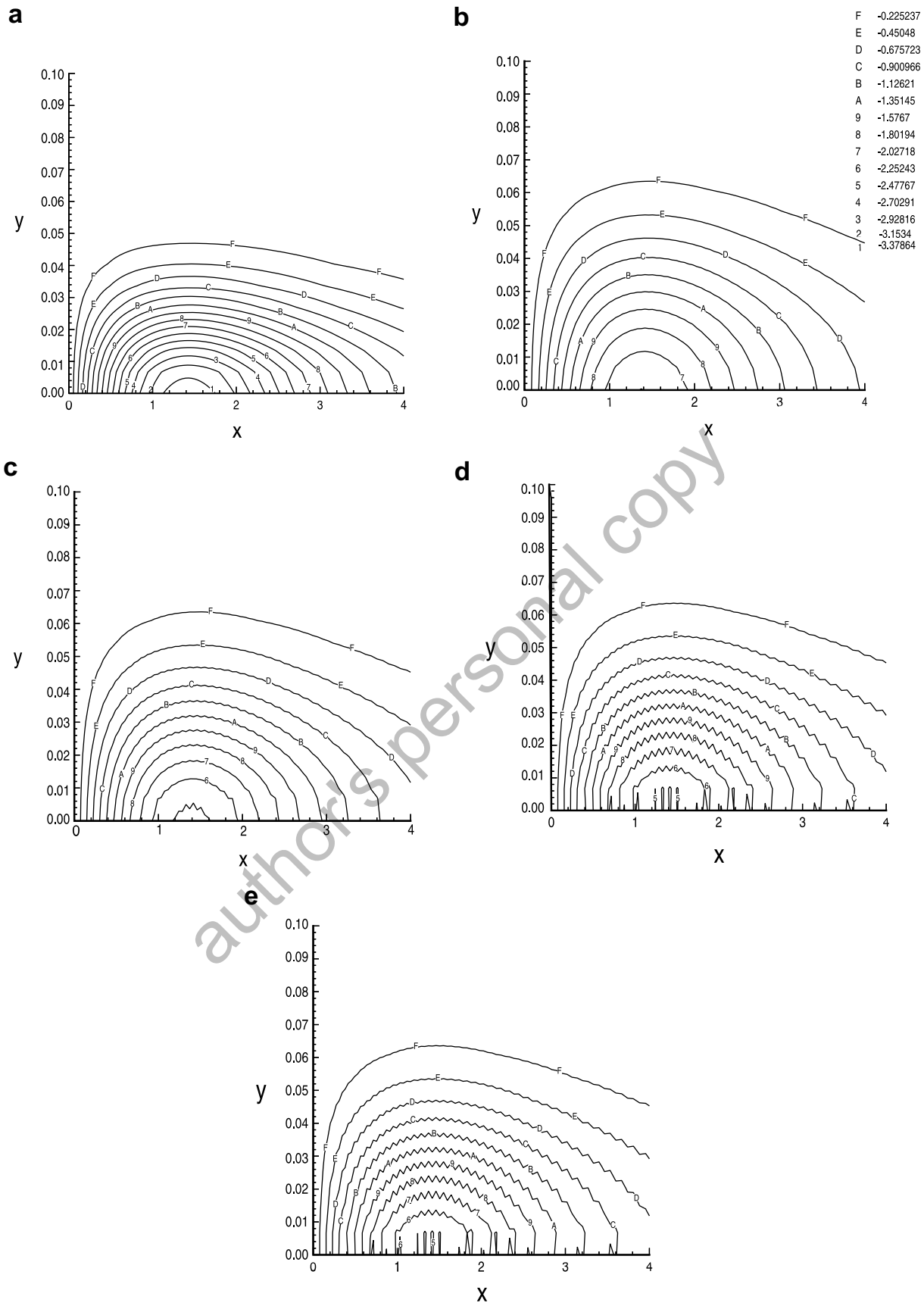

Fig. 3. Vorticity contours near the wall boundary. (a) Initial asymptotic solutions. (b) Ten time step marching using (15) as wall boundary condition. (c) Using Eq. (25) as wall boundary condition. (d) Using Eq. (26) as wall boundary condition. (e) Using Eq. (27) as wall boundary condition.

listed in [9], have also been implemented for comparison. A 150×300 numerical grid, as developed in Section 3, is used, with the symmetry plane at $x = 0$. The circulation Reynolds number, $Re = 500$, was used and the time step was chosen as 0.01 for all the cases.

An Oseen [20] vortex,

$$\zeta = \frac{1}{\pi r_c^2} e^{-r^2/r_c^2}, \tag{22}$$

was used as the initial vortex, started at $x_0 = 1$, where r is the distance from the vortex center, which was assumed to have evolved sufficiently to possess a finite vortex core, $r_c = 0.2$, prior to initiation of the numerical computations. The matched asymptotic analytic solutions for initial wall boundary in [21] are employed, which can be expressed as

$$\Psi = \Psi_0(x, y, t) + \epsilon \Psi_1(x, y, t) + O[\epsilon^2], \tag{23}$$

for the outer solution and

$$\psi = 2\epsilon[\psi_0(x, \eta, t) + \epsilon \psi_1(x, \eta, t)] + O[\epsilon^3], \tag{24}$$

for the inner solution, where $\eta = y/2\epsilon$ is the inner stretched vertical coordinate (see [19] for the detail). The computation starts at $t = 0.1$, when the thickness of the boundary layer has increased to include 10 vertical grid points with the current grid (150×300), so that the numerical resolution becomes enough to resolve the initial boundary layer.

For comparison with boundary condition Eq. (15), the first order and two types of second order boundary conditions in [9], given as

$$\zeta_1 = -\frac{2\psi_2}{h_1^2} + O(h_1), \tag{25}$$

$$\zeta_1 = -\frac{8\psi_2 - \psi_3}{2h_1^2} + O(h_1^2), \tag{26}$$

and

$$\zeta_1 = -\frac{3\psi_2}{h_1^2} - \frac{1}{2}\zeta_2 + O(h_1^2), \tag{27}$$

have been tested. The computations were marched 10 time steps to check the behavior of these different boundary conditions. Vorticity contours in a small region very close to the wall, which should be influenced most strongly by the boundary condition, are displayed to show the flow field in detail.

Fig. 3a represents the initial asymptotic solution results. Fig. 3b is the vorticity contours after marching 10 time steps away from Fig. 3a, using (15) as boundary condition. Fig. 3c shows the result for the first order boundary condition, and Fig. 3d and e are the results for the two second order boundary conditions. In comparison with Fig. 3b, Fig. 3c–e all show significant oscillations in the results. It is interesting to note that the two second order boundary conditions give worse

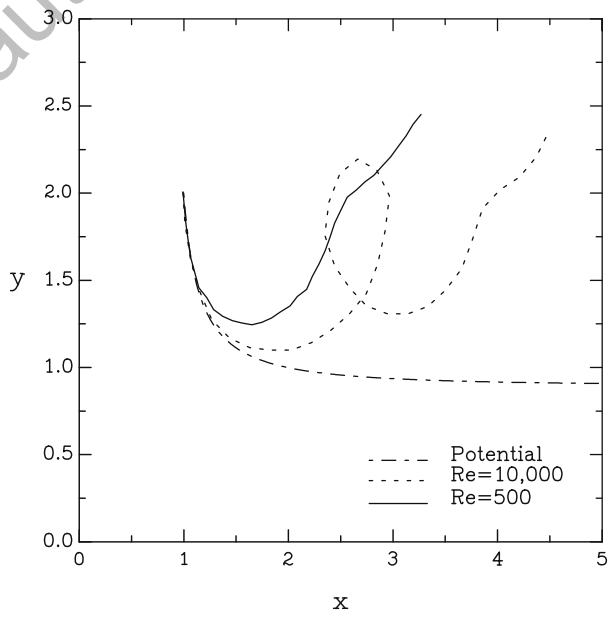

Fig. 4. Vortex trajectories.

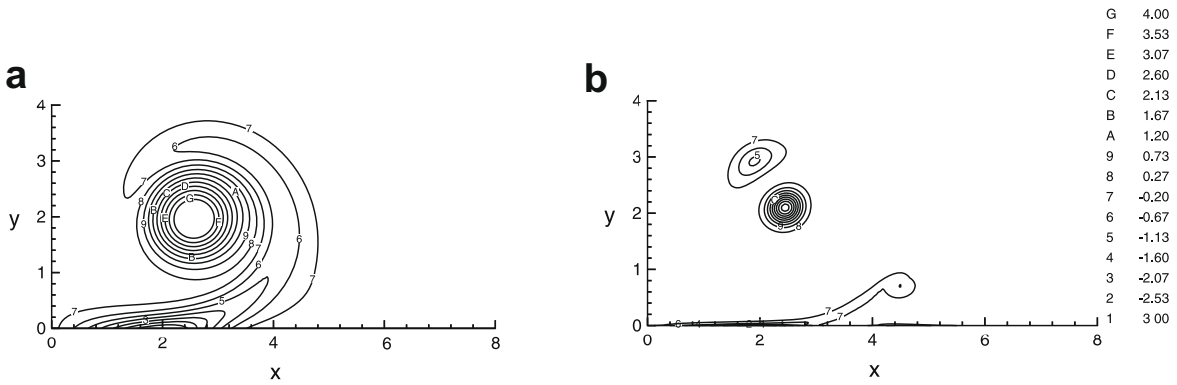

Fig. 5. Vorticity contours. (a) $Re = 500$ and (b) $Re = 10,000$.

results than the first order one. The boundary condition, Eq. (15), mentioned in [9] as the zeroth order vorticity boundary condition, shows the best result of all.

Thereafter, the asymptotic initial solutions and the solid wall boundary condition (15) are then used to simulate the vortex pair interacting with a no-slip solid wall. Fig. 4 shows the trajectories of the right vortex under two different vortex Reynolds numbers, $Re = 500$ and $Re = 10,000$, along with the potential theory result. The potential theory result is an analytical solution for a pair of potential vortices with its image reflecting from the other side of the wall, in order to satisfy the non-penetration boundary condition (the no-slip boundary condition cannot be accommodated by the inviscid solution). The total simulation time is 180 dimensionless time units, defined as s_0^2/Γ_0 At the early time levels, before the vortex approaches close to the wall, the trajectories for the two viscous cases are almost identical and are very close to the inviscid result. Before rebound, the higher Re number trajectory follows closer to the inviscid model and approaches closer to the wall. When rebound starts, the vortex in the higher Reynolds number case rebounds more quickly, while the lower Reynolds number case shows more viscous retardation. The dramatic difference between the trajectories of the two viscous cases after rebound, is due to the generation of secondary vortices near the boundary, as shown in Fig. 5. While there are two secondary vortices generated in the $Re = 10,000$ case which causes a looping in the trajectory, only one secondary vortex is shown in the $Re = 500$ case, due to greater viscous diffusion. The rebound mechanism shown here is in agreement with the experimental description of [2]. It should be noted further that multiple rebound phenomena to result from interactions with multiple secondary vortices, as predicted in [20], were not predicted in the current computations at similar Reynolds numbers.

5. Conclusion

A mathematically and physically consistent boundary condition has been derived for the vorticity–streamfunction formulation. Consistency of the boundary condition assures that fine grid mesh can be used to increase the accuracy of the computation. Therefore, although the boundary condition itself is only first order accurate in terms of the grid size on the wall surface, the fact that fine resolution grids are generally used in the near wall region merits a first order accurate boundary condition. In combining with the asymptotic expansion solutions for the initial conditions, numerical test cases show better results with the present boundary condition than those with the vorticity–streamfunction boundary conditions in the literature, even though the latter have a nominal higher order accuracy in their expressions.

Acknowledgement

The author is grateful for the discussion and advice from Dr. R.L. Ash at Old Dominion University.

References

[1] T.L. Doligalski, C.R. Smith, J.D.A. Walker, Vortex interactions with walls, Annu. Rev. Fluid Mech. 26 (1994) 573–616.
[2] J.K. Harvey, F.J. Perry, Flowfield produced by trailing vortices in the vicinity of the ground, AIAA J. 9 (1971) 1600–1659.
[3] P.M. Gresho, Incompressible fluid dynamics: some fundamental formulation issues, Annu. Rev. Fluid Mech. 23 (1991) 413–453.
[4] P.M. Gresho, Some current CFD issues relevant to the incompressible Navier–Stokes equations, Comput. Methods Appl. Mech. Eng. 87 (1991) 201–252.
[5] P.M. Gresho, Some interesting issues in incompressible fluid dynamics, both in the continuum and in numerical simulation, Adv. Appl. Mech. 28 (1991) 46–141 (Edited by J.W. Hutchinson, T.Y. Wu).
[6] C.R. Anderson, Vorticity boundary conditions and boundary vorticity generation for two-dimensional viscous incompressible flows, J. Comput. Phys. 80 (1989) 72–97.
[7] M.M. Gupta, R.P. Manohar, Boundary approximations and accuracy in viscous flow computations, J. Comput. Phys. 31 (1979) 265–288.
[8] H.J. Lugt, Y. Rimon, Finite-difference approximations of the vorticity of laminar flows at solid surface, Naval Ship Res. Dev. Ctr. Rep. 3306 (1970).
[9] S.A. Orszag, M. Israeli, Numerical simulation of viscous incompressible flows, Annu. Rev. Fluid Mech. 6 (1974) 281–318.
[10] L. Quartapelle, Vorticity conditioning in the computation of two-dimensional viscous flows, J. Comput. Phys. 40 (1981) 453–477.
[11] A.J. Chorin, Numerical study of slightly viscous flow, J. Fluid Mech. 57 (1973) 785–796.
[12] C.R. Anderson, Observations on vorticity boundary conditions, in: R.E. Caflisch (Ed.), Mathematical Aspects of Vortex Dynamics, SIAM, 1989.

[13] A.J. Bilanin, M.E. Teske, C. du P. Donaldson, G.G. Williamson, Vortex interactions and decay in aircraft wakes, NASA Contractor Report, NASA CR-2870, 1977.
[14] L. Ting, On the application of the integral invariants and decay laws of vorticity distributions, J. Fluid Mech. 127 (1983) 497–506.
[15] A.J. Peace, N. Riley, A viscous vortex pair in ground effect, J. Fluid Mech. 129 (1983) 409–426.
[16] A. Arakawa, Computational design for long-term numerical integration of the equations of fluid motion: two-dimensional incompressible flow. Part I, J. Comput. Phys. 1 (1966) 119–143.
[17] B.P. Leonard, A stable and accurate convective modelling procedure based on quadratic upstream interpolation, Comput. Methods Appl. Mech. Eng. 19 (1979) 1600–1659.
[18] P.N. Swarztrauber, R.A. Sweet, Algorithm 541, Efficient FORTRAN subprograms for the solution of separable elliptic partial differential equations [D3], ACM Trans. Math. Software 5 (1979) 352–364.
[19] Z.C. Zheng, The influence of Reynolds number and atmospheric effects on aircraft wake vortices near the ground, Ph.D. Dissertation, Old Dominion University, Norfolk, VA, 1993.
[20] C.W. Oseen, Uber wirbelbewegung in einer meibenden flussigkeit, Arkiv Fur Mathematic Astronomi Och Fysik 7 (1911) 1–13.
[21] P. Orlandi, Vortex dipole rebound from a wall, Phys. Fluids A 2 (1983) 1429–1439.